ACS APPLIED MATERIALS & INTERFACES

www.acsami.org

Research Article

Directional Water Transfer Janus Nanofibrous Porous Membranes for Particulate Matter Filtration and Volatile Organic Compound Adsorption

Wenshi Xu, Yong Chen, and Yu Liu*

Cite This: *ACS Appl. Mater. Interfaces* 2021, 13, 3109−3118

Read Online

ACCESS | Metrics & More | Article Recommendations | Supporting Information

ABSTRACT: In order to reduce the possible harm caused by air pollution, excellent personal protective materials are attracting more and more attention. Therefore, the research of multifunctional materials that can filter particulate matter (PM) and volatile organic compounds (VOCs) simultaneously is of great significance. In addition, in cold weather, water vapor in the exhaled gas condenses into small droplets inside the respirator causing uncomfortable feeling of dampness. Herein, we prepared several types of cyclodextrin-containing Janus nanofibrous porous membranes by electrospinning, which can efficiently filter PM of different sizes in the air, effectively adsorb VOCs, and orientate moisture from exhaled gas to the outside of the membranes to provide a dry and comfortable environment. These advantageous features, combined with the cheap price and easy availability of component materials and low respiratory resistance, highlight the great potential of these Janus nanofibrous porous membranes in the development of personal wearable air purifiers.

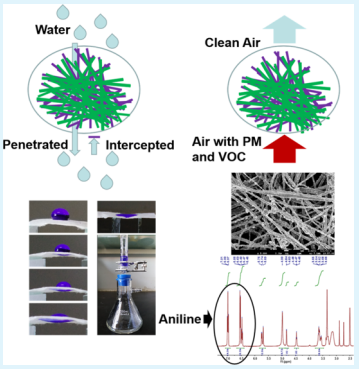

KEYWORDS: *directional water transfer, PM filtration, VOC adsorption, Janus nanofibrous porous membranes, electrospinning*

INTRODUCTION

Air pollution affects the environment and climate and endangers the safety of human beings and other organisms.[1−4] Studies have shown that air pollution may induce a variety of diseases such as respiratory,[5,6] cardiovascular,[7,8] Alzheimer's,[9] and even cancer[10−12] or aggravate these diseases. In recent years, particulate matter (PM), one of the main pollutants in the atmosphere, has attracted considerable attention. Therefore, personal protective materials with good PM filtration performance have become a research hotspot. An electrospinning technology can spin a wide variety of polymers with a controllable technology. The obtained nanofibrous membrane has small fiber diameter, high porosity, good fiber uniformity, and light weight. Compared with common filter membranes, the air permeability is higher under the same filtering effect. Electrospinning produces nanofibers with controlled size, morphology, and functional groups.[13] The resulting fibrous membranes have high PM removal efficiency and low airflow resistance, making them ideal candidate for air filtration applications. Therefore, polymers such as polyacrylonitrile (PAN),[14,15] polycarbonate,[16] chitosan,[17] polycaprolactone (PCL),[18] polyethylene oxide,[19] and polyurethane[20] have been used to prepare electrospun membranes as air filter. Dipole−dipole or induced dipole interactions can enhance the binding of PM with the surface of nanofibers, and PAN is considered as a good material for filtering PM because of its large dipole moment.[21] Besides PM, volatile organic compounds (VOCs) are also main components of atmospheric pollutants. VOC exposure can lead to dyspnea, eye and throat irritation, and cancer.[22] Therefore, the research of multifunctional materials that can filter PM and VOC simultaneously is of great significance. Based on the host−guest interaction, the research and application range of macrocyclic compounds is very wide, including chiral recognition,[23] optical properties,[24−26] catalysis,[27,28] nanocarriers,[29,30] adsorption, and separation.[31,32] On the other hand, most commercial masks are made of hydrophobic materials. When the temperature is low, the water vapor in the exhaled gas condenses into small droplets inside the respirator. The hydrophilic materials can absorb the water drop but keep them on the materials. Therefore, both hydrophobic and hydrophilic materials cause uncomfortable feeling of dampness. The comfort of masks is also an important aspect which should be paid more attention. Therefore, there is an urgent need for a mask that can direct exhale water vapor or water droplets to the outside of the mask.

Janus membranes can solve the above problems well. The front and back sides of Janus membranes have different wettability and are used for directional transportation of water

Received: October 15, 2020
Accepted: December 4, 2020
Published: January 8, 2021

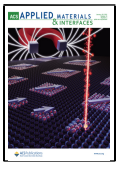

Scheme 1. Schematic Diagram of PAN/β-CD/PCL/ZnO and PAN/β-CD/11% PCL/2% PCL Janus Nanofibrous Membranes Prepared by Electrospinning Technology and Their Application in PM, VOC Filtration, and Directional Water Delivery; Purple Fibers Represent PAN/β-CD Hydrophilic Layer, Green Fibers Represent PCL/ZnO or 11% PCL/2% PCL Hydrophobic Layer

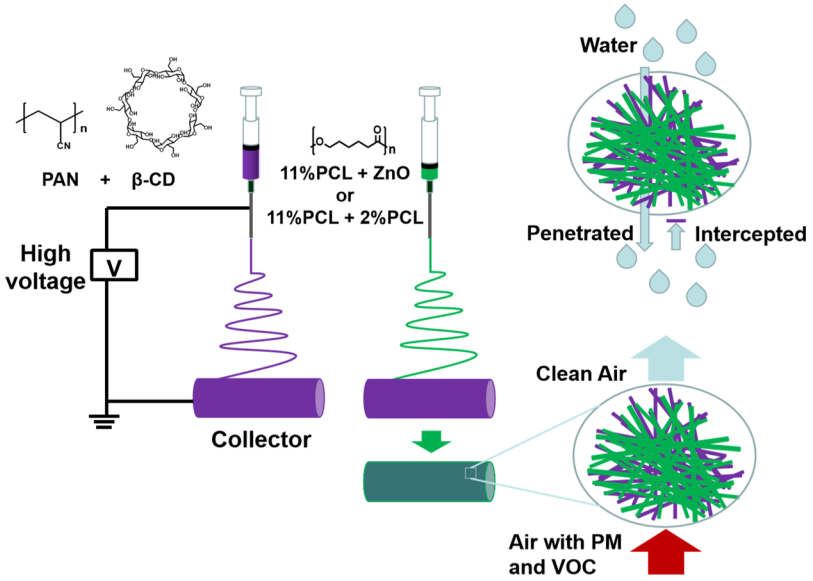

or oil. Wang et al. reported a fibrous membrane with different wettability on the two sides that was superhydrophobic and oleophilic on the PVDP-HFP side but superamphiphobic on the PVDF-HFP/FD-POSS/FAS side, which allowed unidirectional oil-transport just from the PVDF-HFP/FD-POSS/FAS to the PHVF-HFP side.[33] In addition to the unidirectional oil-transport ability, several materials with asymmetric wettability also show their unique capability to transfer water droplet. Shi et al. reported a self-pumping dressing that could unidirectionally drain the excessive biofluid from its hydrophobic side to hydrophilic side, thereby preventing the biofluid from wetting the wound.[34] Dai et al. reported a Janus polyester/nitrocellulose textile with conical micropores that could weaken undesired wet adhesion and heat loss because of the removal of liquid.[35] Inspired by these findings, it is believed that the Janus membrane can well solve the discomfort caused by the exhaled water vapor condensation into the face.

Herein, we prepared three Janus nanofibrous porous membranes by electrospinning. The hydrophilic sides of the three Janus membranes are all PAN nanofibers containing 50% β-cyclodextrin, while the hydrophobic sides are 11% PCL/hydrophobic zinc oxide(ZnO), 11% PCL/2% PCL, and a hydrophobic layer stripped from the middle of a commercial mask, respectively. The hydrophobic layer is doped with hydrophobic zinc oxide or 2% PCL in order to increase the roughness and enhance the hydrophobicity. When used as a mask, the hydrophobic side of the Janus membrane fits over the face and the hydrophilic side faces outward. The water vapor or condensed water droplets exhaled by the human body can be directed to the outside of the mask to reduce the uncomfortable feeling of dampness. At the same time, the hydrophilic layer containing PAN and β-cyclodextrin can effectively intercept PM and VOC (Scheme 1).

EXPERIMENTAL SECTION

Materials. PAN (M_w = 150 kDa) was purchased from Heowns Biochem LLC. *N*,*N*-Dimethylformamide was purchased from Concord Technology (Tianjin) Co., Ltd. β-Cyclodextrin was purchased from Kmart (Tianjin) Chemical Technology Co., Ltd. PCL (M_w = 80 kDa) was purchased from Dalian Meilun Biotechnology Co., Ltd. Hexafluoroisopropanol was purchased from Heowns Biochem Technologies LLC. Organosilane-covered hydrophobic zinc oxide was purchased from Energy Chemical. All chemicals and solvents were used without further purification.

Preparation of Janus Nanofibrous Membranes. The 12 w/v % PAN solution containing 50% β-cyclodextrin was transferred to a 5 mL syringe with a 23 gauge needle tip, and the spinning flow rate was 0.3 mm/min. A high voltage of 25 kV was applied, and the distance between the collector coated with aluminum foil and the needle tip was 20 cm. The collector was rotated at 40 rpm. After 5 mL of PAN/β-CD was electrospinned, 1 mL of 11 w/v % PCL solution containing 27% ZnO was electrospinned on it under the same spinning conditions. Dry PAN/β-CD/PCL/ZnO Janus nanofibrous membrane was collected directly from the aluminum foil-covered collector and stored at room temperature. For the PAN/β-CD/11% PCL/2% PCL Janus nanofibrous membrane, after 5 mL of PAN/β-CD was electrospinned, 1 mL of 11 w/v % PCL solution and 1 mL of 2w/v % PCL solution were electrospinned on it under the same spinning conditions. For the PAN/β-CD/mask Janus nanofibrous membrane, the 12 w/v % PAN solution containing 50% β-cyclodextrin was electrospinned on the collector coated with the aluminum foil-covered commercial mask.

Characterization of Janus Nanofibrous Membranes. Scanning electron microscopy (SEM, MERLIN Compact, Germany) was used to inspect the surface microstructure of the nanofibrous membranes. All membranes were vacuum-dried and then coated with a thin layer of gold to increase their conductivity. The SEM images were captured using a detector with an acceleration voltage of 2 kV. A Fourier transform infrared spectrometer (FTIR) (Bruker-TENSOR II, Germany) was used to obtain the infrared spectra of samples between 4000 and 400 cm^{-1}. An optical contact angle (CA) meter (DSA100, Germany) was used to measure the water CA at ambient conditions. In detail, the membranes were cut into rectangular blocks (1 × 1 cm^2) and placed in a vacuum oven overnight. A water droplet (3 μL) was dropped on the surface of the membranes, and the CA value was obtained. For each test, three samples were used as a parallel control. X-ray diffraction (XRD) patterns were measured on a Rigaku SmartLab (Japan) diffractometer using Cu Kα radiation. The mechanical stability of the nanofibrous membranes was measured using a universal tensile tester (Instron-

https://dx.doi.org/10.1021/acsami.0c18526
ACS Appl. Mater. Interfaces 2021, 13, 3109−3118

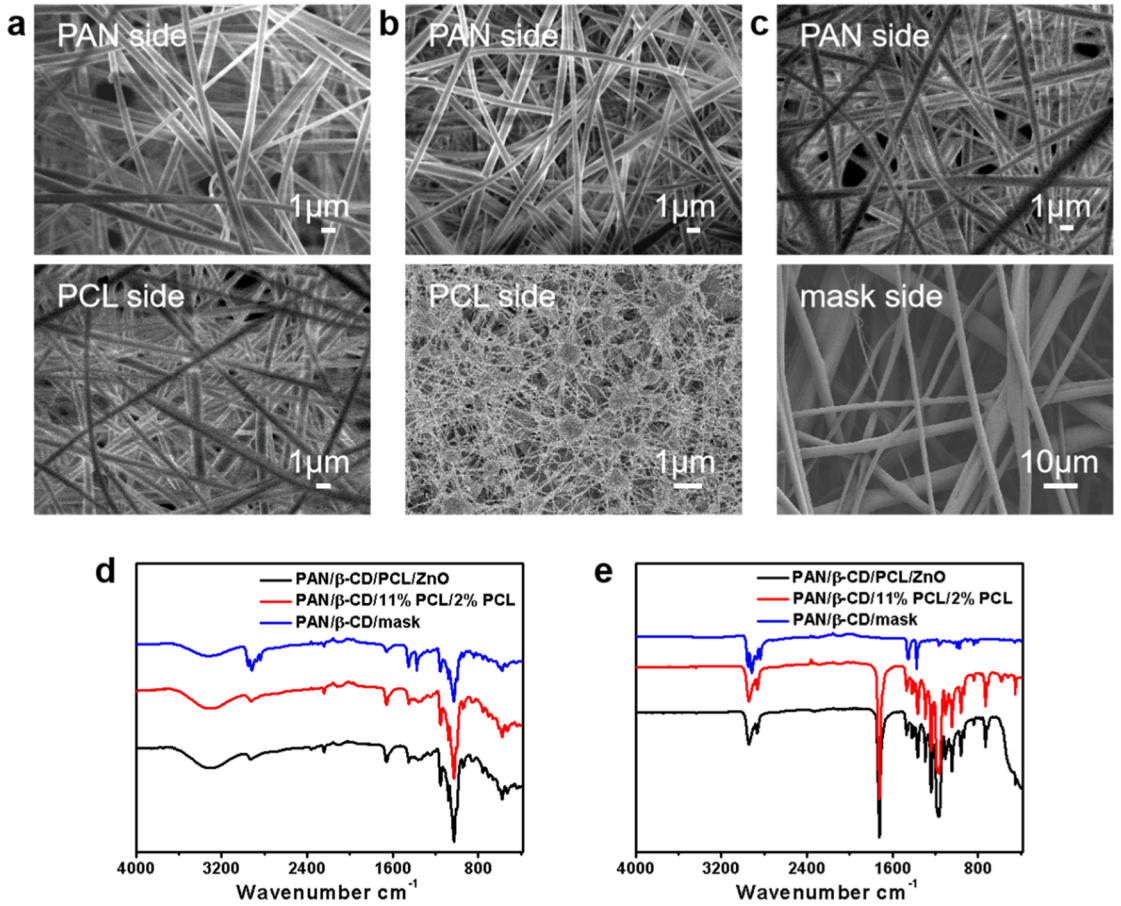

Figure 1. Characterization of the three Janus nanofibrous membranes. SEM images of electrospun fibers of (a) PAN/β-CD/PCL/ZnO, (b) PAN/β-CD/11% PCL/2% PCL, and (c) PAN/β-CD/mask. The top pictures are the hydrophilic side, and the bottom pictures are the hydrophobic side. FTIR spectra of (d) hydrophilic side and (e) hydrophobic side of PAN/β-CD/PCL/ZnO, PAN/β-CD/11% PCL/2% PCL, and PAN/β-CD/mask.

336, USA) with load cell capacity of 10 N. The nanofibrous membranes were sectioned into rectangular strips of 4 × 1 cm^2 (length × width), which were then fixed to the grips of the tester and permitted to elongate at an extension speed of 100 mm/min, until they snapped. The nitrogen adsorption isotherms and pore size distributions of the membranes were measured using an automatic gas adsorption analyzer (Autosurb IQ, USA). The Brunauer–Emmett–Teller (BET) equation was used for determining the surface area from the nitrogen adsorption isotherms at liquid nitrogen temperatures.

PM Filtration Efficiency and Pressure Drop of Janus Nanofibrous Membranes. The concentration and size distribution of PM in the presence or absence of Janus nanofibrous membranes were detected by a hand-held condensation particle counter (CPC, TSI model 3007, USA) used to detect PM greater than 10 nm, a scanning mobility particle sizer (SMPS, TSI model 3936, USA) used to detect PM between 14.6 and 660 nm, and an optical particle sizer (OPS, TSI model 3330, USA) used to detect PM between 300 and 10,000 nm. The main difference among CPC3007, SMPS, and OPS instruments is that the size range of PM they detect is different. The use of three instruments at the same time plays a complementary role. The air filtration efficiency was calculated as $1 - C/C_0$, where C and C_0 are the concentrations of PM with and without the filters, respectively. The pressure drop (p), representing the resistance across the Janus nanofibrous membranes, was measured by a differential manometer.

VOC Adsorption of Janus Nanofibrous Membranes. The evaluation of the adsorption performance of Janus membranes for VOC is carried out with aniline vapor as an example. In detail, 10 mL of aniline was put into a desiccator with a diameter of 15 cm. About 50 mg of Janus membranes were placed into the desiccator and sealed with vacuum grease. After 2 days of exposure in an aniline atmosphere, the Janus membranes were taken out. The examination of the aniline adsorption capacity was carried out by proton magnetic resonance (^{1}H NMR), ultraviolet–visible spectroscopy (UV–vis), and directly weighing the Janus membranes before and after aniline exposure. After adsorption of aniline, 20 mg of Janus membranes (PAN/β-CD/PCL/ZnO, PAN/β-CD/11% PCL/2% PCL, and PAN/β-CD/mask) were dissolved in 600 μL of DMSO-d_6 for NMR detection. ^{1}H NMR spectra were recorded on a Bruker AVANCE AV400 (400 MHz). However, in order to facilitate quantification, about 15 mg of Janus membranes (PAN/PCL/ZnO, PAN/11% PCL/2% PCL, and PAN/mask) adsorbed with aniline were dissolved in 600 μL of DMSO-d_6, and then, about 10 mg of β-cyclodextrin was added for NMR detection. The molar ratios between aniline and β-cyclodextrin were determined by integrating the peak of the characteristic chemical shifts (δ) corresponding to aniline and β-cyclodextrin. The amount of β-cyclodextrin is known, so the amount of aniline adsorbed can be calculated. The procedure for calculating the adsorption capacity of aniline by UV absorption spectrum is as follows: 15 mg of Janus membranes adsorbed with aniline were dissolved in 3 mL of dimethyl sulfoxide (DMSO), and the ultraviolet absorption spectra were measured. By comparing the standard curve of aniline, the concentration of aniline in the sample can be known, and the amount of adsorbed aniline can be further calculated.

RESULTS AND DISCUSSION

Characterization of Janus Nanofibrous Membranes. Figure 1a–c presents the SEM images of the three Janus nanofibrous membranes prepared by electrospinning. The hydrophilic PAN sides of these three Janus nanofibrous membranes were smooth and uniform nanofibers with an

https://dx.doi.org/10.1021/acsami.0c18526
ACS Appl. Mater. Interfaces 2021, 13, 3109–3118

average diameter of about 580 nm. The hydrophobic PCL side of PAN/β-CD/PCL/ZnO were smooth and uniform nanofibers with a diameter of 560 nm. The hydrophobic PCL side of PAN/β-CD/11% PCL/2% PCL could not form smooth nanofibers because the concentration of 2% PCL was too low and the molecular chains were less entangled in the solution. Instead, nanofibers with a large number of beads were formed. The average diameter of the fibers was only 80 nm. The hydrophobic mask side of the PAN/β-CD/mask was a hydrophobic layer stripped from the middle of a commercial mask with a wide fiber diameter range from 1.45 to 7.6 μm and an average diameter of 3.37 μm. Figure 1d,e shows the FTIR spectrum of the three Janus nanofibrous membranes. As shown in Figure 1d, the characteristic absorption peaks of cyano (−CN) appear at 2242 cm^{-1}, and the characteristic absorption peaks of $-CH_2$ at 2923 and 1452 cm^{-1} indicated the successful construction of PAN nanofibers. Moreover, the peak at 3307 cm^{-1} was assigned to the stretching vibration peak of −OH, and the peaks in the 1200−1000 cm^{-1} region were the characteristic peaks of the glucose ring, which proved that β-cyclodextrin was contained in the nanofibers. This confirms that the hydrophilic sides of all of the three Janus membranes are PAN/β-CD nanofibers. As shown in Figure 1e, the peaks at 2944 and 2865 cm^{-1} were assigned to the stretching vibration peaks of C−H, the peak at 1722 cm^{-1} was assigned to C═O, the peaks in the 1471−1365 cm^{-1} region were assigned to the bending vibration of C−H, and the peaks in the 1294−1165 cm^{-1} region were the characteristic peaks of C−O−C. The above result indicated the successful construction of PCL nanofibers. For the hydrophobic side of PAN/β-CD/PCL/ZnO, in addition to the characteristic peaks of PCL, the peak at 453 cm^{-1} was assigned to ZnO. As shown in Figure 1e, for the hydrophobic side of the PAN/β-CD/mask, the peaks at 2950 cm^{-1} and 2917 cm^{-1} were assigned to the asymmetric stretching vibration peak of $-CH_3$ and $-CH_2$, the peaks at 2867 and 2837 cm^{-1} were assigned to the symmetric stretching vibration peak of $-CH_3$ and $-CH_2$, the peaks at 1454 and 1376 cm^{-1} were assigned to the asymmetric and symmetric deformation vibration peaks of $-CH_3$, and the peaks at 1166, 997, 899, and 841 cm^{-1} were isotactic polypropylene (PP) absorption bands. The above results prove that the material constituting the mask is PP. As shown in Figure 1d, the characteristic peaks of PP appeared in the hydrophilic side of the PAN/β-CD/mask may be due to the fact that the hydrophobic mask layer was detected through the pores of the hydrophilic layer in the process of infrared detection.

As shown in Figure 2, all of the three Janus membranes showed significant wettable anisotropy to water on their two sides. Their water CAs are shown in Figure 2a. The water CAs of the hydrophilic side and the hydrophobic side were 24.6 and 125.6° for PAN/β-CD/PCL/ZnO, 17.4 and 118.1° for PAN/β-CD/11% PCL/2% PCL, and 41.7 and 133.1° for the PAN/β-CD/mask. From the optical images (Figure 2b) and photographs taken by the mobile phone (Figure 2c) of a water droplet on the hydrophilic side and the hydrophobic side of PAN/β-CD/PCL/ZnO, PAN/β-CD/11% PCL/2% PCL, and PAN/β-CD/mask, the difference of wettability between the two sides could also be observed.

It can be seen from Figure S1a that the PAN/β-CD/PCL/ZnO Janus membrane has a diffraction peak at 2θ = 17°, belonging to the (100) crystal plane, and is also a characteristic diffraction peak of the cyano group. The diffraction peaks at 2θ = 21.4 and 23.8° belong to PCL, and diffraction peaks at 2θ =

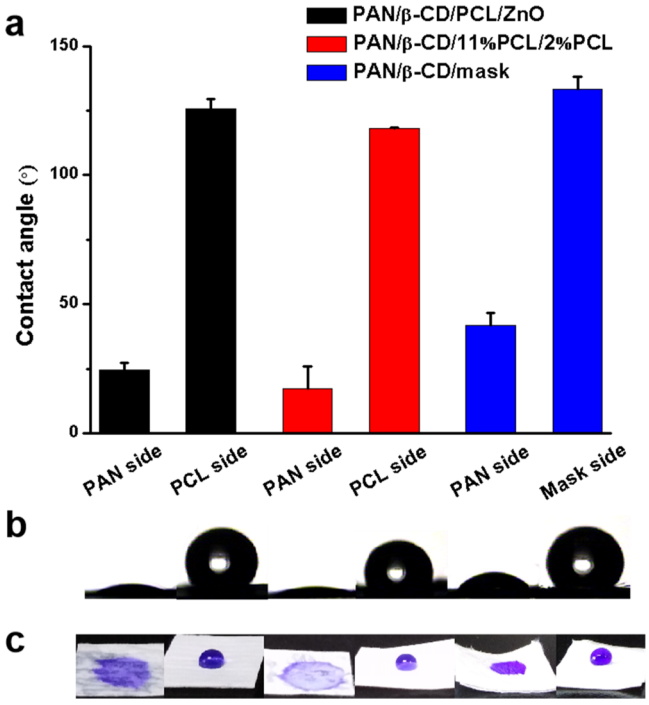

Figure 2. (a) CA quantitative data, (b)optical images, and (c) photographs taken by the mobile phone of the hydrophilic side and the hydrophobic side of PAN/β-CD/PCL/ZnO, PAN/β-CD/11% PCL/2% PCL, and PAN/β-CD/mask.

31.7, 34.4, 36.3, 47.5, and 56.6° belong to ZnO. PAN/β-CD/11% PCL/2% PCL exhibits a characteristic diffraction peak of PAN at 2θ = 17° and characteristic diffraction peaks of PCL at 2θ = 21.4 and 23.8° (Figure S1b). The PAN/β-CD/mask exhibits characteristic diffraction peaks of PP at 2θ = 14.2, 16.9, and 18.6°, and the characteristic diffraction peak of PAN at 2θ = 17° is overlapped with the characteristic peak of PP at 16.9° (Figure S1c).

In the application of electrospun Janus membranes, mechanical property is an important factor. Figure S2 shows the stress−strain curves of PAN/β-CD/PCL/ZnO, PAN/β-CD/11% PCL/2% PCL, and PAN/β-CD/mask. The PAN/β-CD/PCL/ZnO Janus membrane showed an average yield strength of 3.094 MPa and the elongation at break of 59.662%. The PAN/β-CD/11% PCL/2% PCL Janus membrane showed an average yield strength of 5.518 MPa and the elongation at break of 60.835%. The PAN/β-CD/mask Janus membrane showed an average yield strength of 3.128 MPa and the elongation at break of 6.56%. These membranes exhibited a plastic behavior and could undergo significant deformation not a sudden breakage during stretching. Their mechanical property is similar or even better than other electrospun membranes.[18,36]

The surface areas of the Janus membranes were determined using nitrogen adsorption isotherms, where PAN/β-CD/PCL/ZnO, PAN/β-CD/11% PCL/2% PCL, and PAN/β-CD/mask exhibited BET surface areas of 10.089, 8.364, and 6.796 m^2/g, respectively (Figure S3a−c). Pore size distributions of the three Janus membranes indicated that the measured Janus membranes contain micropores, mesopores, and macropores with a large porosity (Figure S3d−f). Because of the small fiber diameter and many pores of the electrospun Janus membranes, the surface area is large, which is conducive to the filtration of PM and VOC.

https://dx.doi.org/10.1021/acsami.0c18526
ACS Appl. Mater. Interfaces 2021, 13, 3109−3118

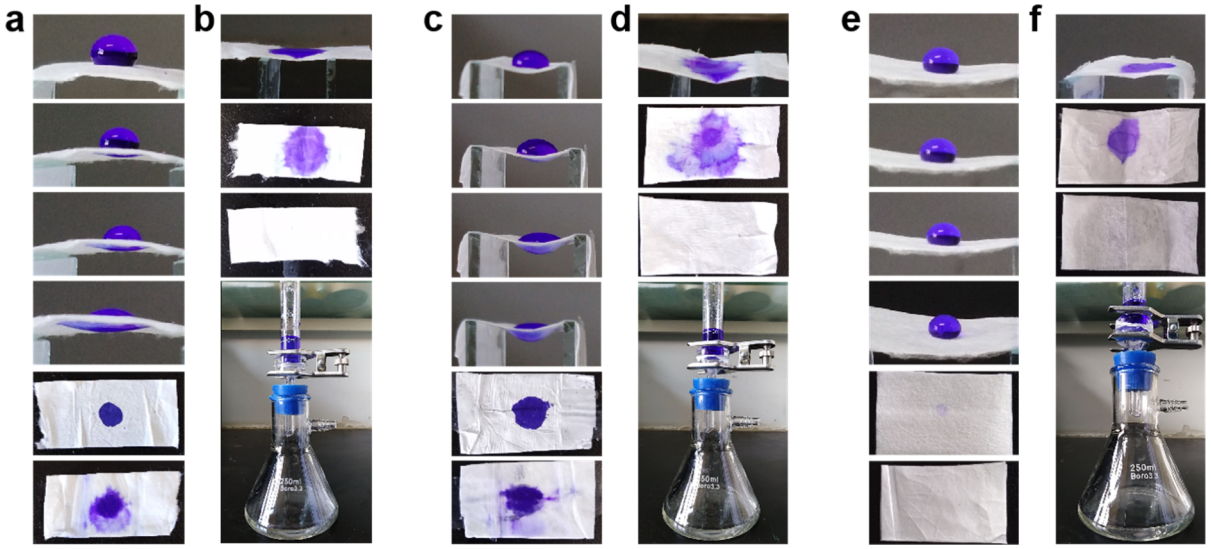

Figure 3. Water unidirectional penetration of the Janus membranes. (a) Water dyed by ethyl violet could easily penetrate the PAN/β-CD/PCL/ZnO Janus membrane from hydrophobic PCL/ZnO to hydrophilic PAN/β-CD direction. (b) Water is blocked on the Janus membrane from hydrophilic PAN/β-CD to hydrophobic PCL/ZnO direction. (c) Water could penetrate the PAN/β-CD/11% PCL/2% PCL Janus membrane from hydrophobic 11% PCL/2% PCL to hydrophilic PAN/β-CD direction. (d) Water is blocked on the Janus membrane from hydrophilic PAN/β-CD to hydrophobic 11% PCL/2% PCL direction. Water is blocked on both the (e) hydrophobic side and (f) hydrophilic side of the PAN/β-CD/mask Janus membrane.

Water Unidirectional Penetration of Janus Nanofibrous Membranes. The anisotropic Janus membranes show great water unidirectional penetration performance (Figure 3). We use ethyl violet dyed water instead of water in order to observe the unidirectional permeability of the Janus membranes more clearly and intuitively. Taking the PAN/β-CD/PCL/ZnO membrane as an example, water stained by ethyl violet could penetrate the membrane from hydrophobic PCL side to hydrophilic PAN side with low hydraulic pressure and it would not spread in the hydrophobic layer (Figure 3a, Supporting Information, Movie S1). It is reported that the PAN electrospun nanofibrous membrane has certain ethyl violet filtration ability,[13] and the Janus membrane contains PAN electrospun nanofibers. Therefore, the purple aqueous solution becomes colorless after passing through the membrane (Supporting Information, Movie S1). However, on the opposite PAN side to PCL side direction, water droplet spread on the hydrophilic layer, but it could not penetrate the Janus membrane, and at high hydrostatic pressure, 5 mL of water was blocked (Figure 3b, Supporting Information, Movie S2). The hydrophilic PAN layer and hydrophobic PCL layer do not separate from each other during the application process because of the strong electrostatic force during the electrospinning process. Several possible mechanisms have been reported to explain the phenomenon of fluid unidirectional penetration, such as hydrophobic force,[37] Laplace pressure difference,[38] hydrostatic pressure, and capillary force from hydrophilic layer.[34]

Similarly, for the PAN/β-CD/11% PCL/2% PCL Janus membrane, water could penetrate the membrane from hydrophobic PCL side to hydrophilic PAN side (Figure 3c, Supporting Information, Movie S3) but blocked on the opposite PAN side to PCL side direction (Figure 3d, Supporting Information, Movie S4). For the PAN/β-CD/mask Janus membrane, at high hydrostatic pressure, 5 mL of water could penetrate the membrane from hydrophobic mask side to hydrophilic PAN side but blocked on the opposite direction (Supporting Information, Movie S5; Supporting Information, Movie S6). However, at low hydraulic pressure, water droplet was blocked on both sides (Figure 3e,f). The hydrophobic mask layer is a film peeled off from the commercial mask. Its thickness cannot be adjusted, and the hydrophobic layer is too thick to allow water droplets to penetrate. In addition, the hydrophobic mask layer and the hydrophilic PAN layer are not tightly bonded as the other two Janus membranes, making it difficult for water droplets to penetrate the hydrophobic layer into the hydrophilic layer.

In addition to the directional transport performance of water, the dry condition of Janus membranes to wet skin and water vapor permeability were tested. Wetted skin covered with the three Janus membranes became dry after 10 min because of spontaneous directional water transport. However, the wetted skin covered with the hydrophobic mask and hydrophilic PAN was still wet after 10 min (Figure S4a). As shown in Figure S4b, the water vapor transmission rate of PAN/β-CD/PCL/ZnO, PAN/β-CD/11% PCL/2% PCL, PAN/β-CD/mask, mask, and PAN/β-CD was about 0.00765, 0.00758, 0.00785, 0.00724, and 0.00659 g cm^{-2} h^{-1}, respectively. The water evaporation rate of the three Janus membranes was higher than that of the hydrophobic mask and hydrophilic PAN. The result indicates that the Janus membranes have a better promoting effect on water evaporation than the hydrophobic mask and hydrophilic PAN. Therefore, the wearability of Janus membranes is comparable to that of the commercial respirator.

Efficient PM Capture by the Janus Nanofibrous Membranes. The PM filtration experiments were carried out on a haze day, in a real polluted air environment, and all the three Janus nanofibrous membranes were effective in capturing PM (Figures 4, S5, and Table S1). Air flow with PM passes through Janus membranes from hydrophilic PAN sides to hydrophobic sides. As shown in Figure 4a–c, for all of the three Janus membranes after 4 h of PM exposure, many PM particles with different sizes adhered to the surface of the

https://dx.doi.org/10.1021/acsami.0c18526
ACS Appl. Mater. Interfaces 2021, 13, 3109−3118

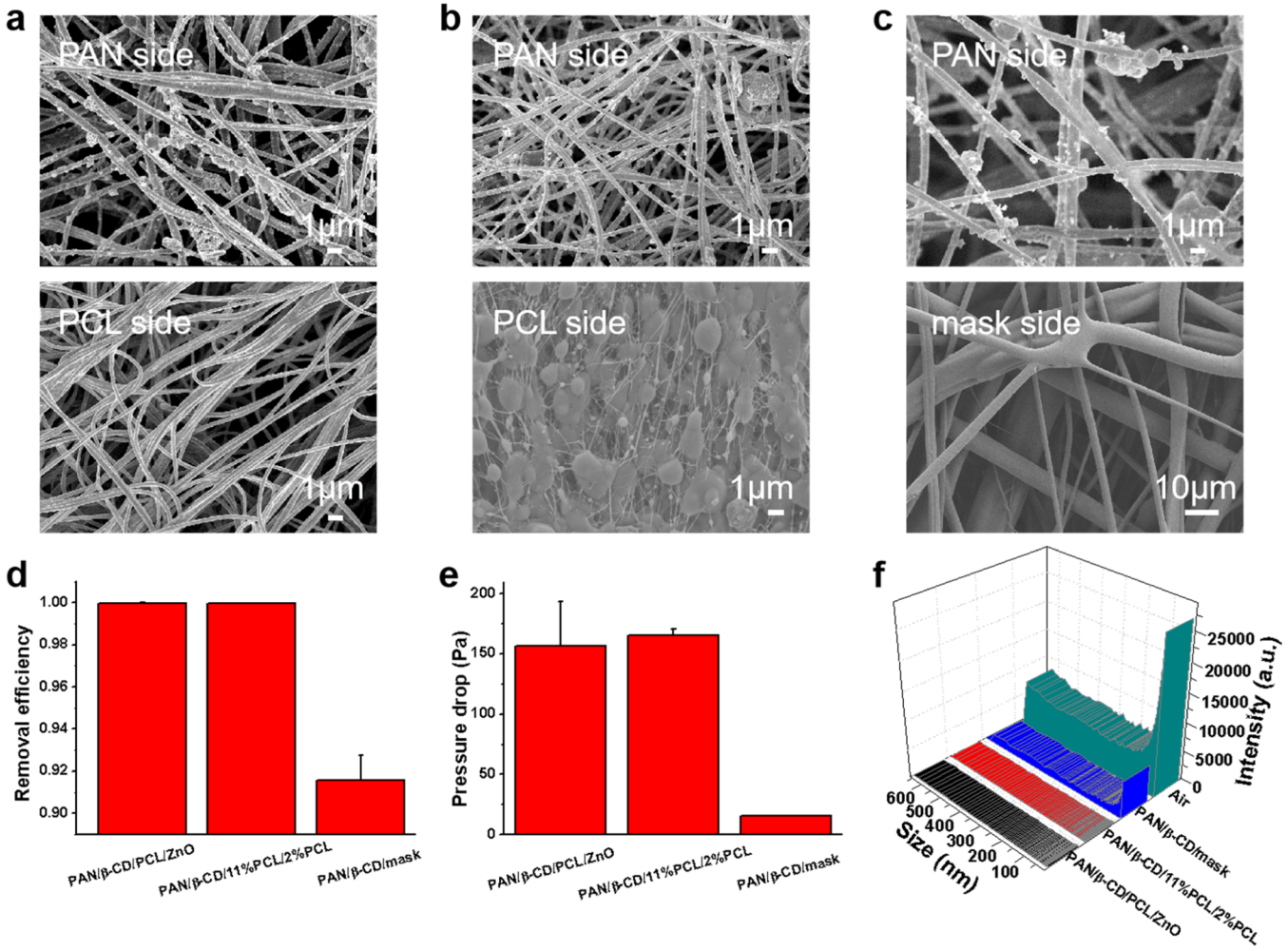

Figure 4. Three Janus membranes filter PM efficiently. SEM images of electrospun fibers of (a) PAN/β-CD/PCL/ZnO, (b) PAN/β-CD/11% PCL/2% PCL, and (c) PAN/β-CD/mask after 4 h PM filtration from the hydrophilic side to hydrophobic side. The top pictures are the hydrophilic side with PM, and the bottom pictures are the hydrophobic side without PM. (d) Removal efficiency of the three Janus membranes measured using hand-held CPC3007. (e) Pressure drop values of the three Janus membranes. (f) SMPS is used to monitor the content of PM with different sizes before and after the filtration of the three Janus membranes in the air.

hydrophilic PAN nanofibers, while PM was not observed on the hydrophobic side, indicating that the Janus membranes could intercept the PM effectively. The concentration and size distribution of the PM particles in the presence or absence of the Janus membranes were detected by handheld CPC3007, SMPS, and OPS instruments. All of the three Janus membranes showed great filtration efficiency of PM. The PM removal efficiency of PAN/β-CD/PCL/ZnO, PAN/β-CD/11% PCL/2% PCL, and PAN/β-CD/mask was 99.99, 99.98, and 91.56%, respectively (Figure 4d). The PAN with a large dipole moment can capture the PM well and tightly bind them through the dipole−dipole or induced dipole interactions. PM filtration efficiency and air permeability are often an opposite relationship, and a balance needs to be found between them. Besides high PM removal efficiency, maintaining good air permeability is very important. A differential pressure gauge was used to measure the pressure difference between the air before and after passing through the Janus membranes. As shown in Figure 4e, the pressure drop of PAN/β-CD/PCL/ZnO, PAN/β-CD/11% PCL/2% PCL, and PAN/β-CD/mask was 156.5, 165.1, and 15.2 Pa, respectively. The pressure drop is lower than 0.2% of atmosphere pressure, which is negligible. In other words, the breathing resistance of Janus membranes used as the mask is very small. The quality factor (QF), defined as $-\ln(1 - E)/\Delta P$ (where E represents the PM removal efficiency and ΔP represents the pressure drop), can be used to assess the overall performance of the Janus membranes, taking both PM removal efficiency and pressure drop into account. The QFs of PAN/β-CD/PCL/ZnO, PAN/β-CD/11% PCL/2% PCL, and PAN/β-CD/mask were 0.05885, 0.05159, and 0.1626 Pa^{-1} (Table S1). The PM removal efficiency was closely related to the BET surface area and microporosity of the Janus nanofibrous membranes. With increasing BET surface area and microporosity, the PM removal efficiency was also improved (Figure S3).

The smaller the particle size of PM, the greater the harm to human health. Therefore, SMPS and OPS equipment were used to measure the removal efficiencies of the Janus nanofiber membranes for PM with different sizes. The results are shown in Figures 4f and S5, respectively. The results show that PAN/β-CD/PCL/ZnO and PAN/β-CD/11% PCL/2% PCL have nearly 100% filtration efficiency for PM with different particle sizes. PAN/β-CD/mask has nearly 100% filtration efficiency for PM larger than 465 nm, and when the PM particle size is smaller than 465 nm, PM filtration efficiency decreases slightly with the decrease of the PM particle size.

https://dx.doi.org/10.1021/acsami.0c18526
ACS Appl. Mater. Interfaces 2021, 13, 3109−3118

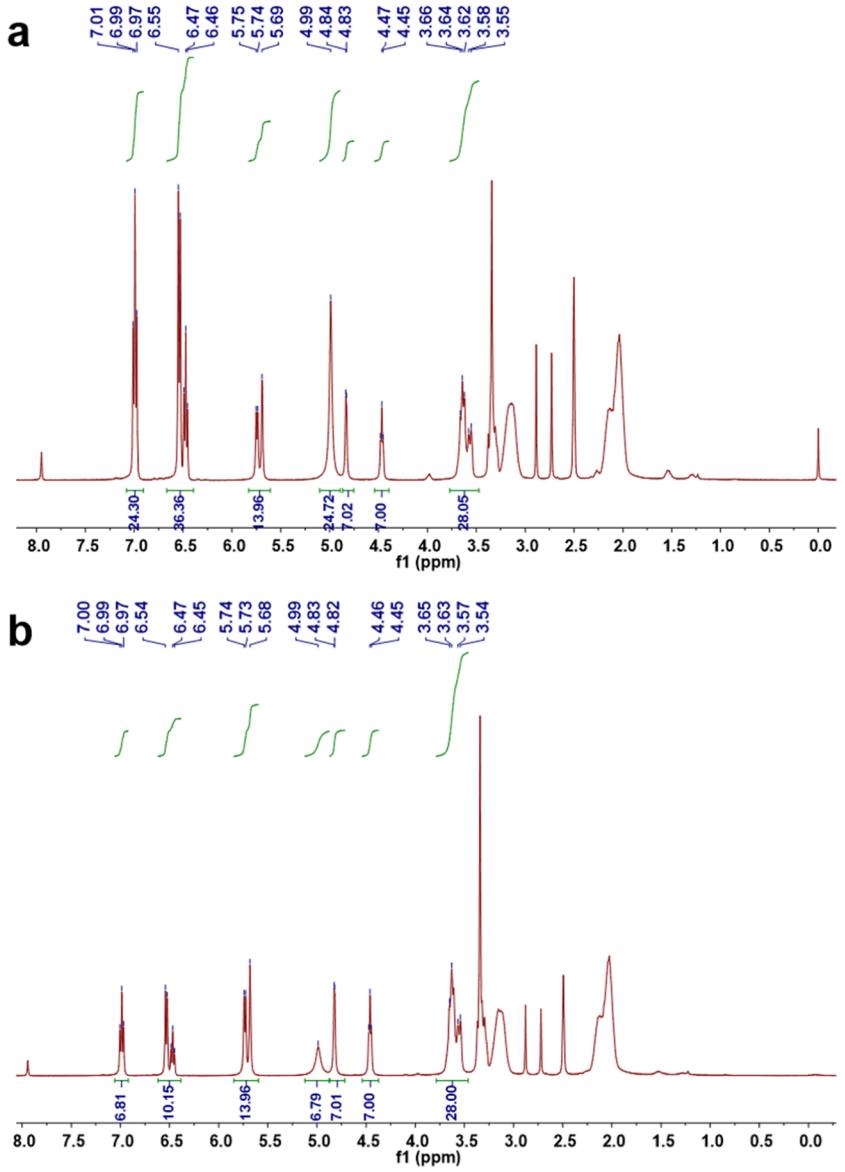

Figure 5. ^{1}H NMR spectra of aniline-exposed (a) PAN/β-CD/11% PCL/2% PCL and (b) PAN/11% PCL/2% PCL in DMSO-d_6.

VOC Adsorption of Janus Nanofibrous Membranes. The VOC adsorption capability of Janus membranes was investigated by using aniline as a model which is known to form an inclusion complex with β-CD.[32] The aniline adsorption capability of Janus membranes was investigated by directly weighing the Janus membranes before and after aniline exposure. The amount of aniline adsorbed by per unit mass of Janus membranes can be calculated by dividing the mass of adsorbed aniline by the mass of the Janus membranes. The results are summarized in Table S2. ^{1}H NMR detection was performed to determine the adsorbed amount of aniline by calculating the molar ratios of aniline and β-CD. ^{1}H NMR spectra of aniline-exposed PAN/β-CD/11% PCL/2% PCL, PAN/11% PCL/2% PCL, PAN/β-CD/PCL/ZnO, PAN/PCL/ZnO, PAN/β-CD/mask, and PAN/mask are shown in Figures 5, S6, and S7.

The molar ratios between aniline and β-cyclodextrin were determined by integrating the peak of the characteristic chemical shifts corresponding to aniline and β-CD. The particular peaks belong to aniline were observed at the aromatic region of NMR spectrum (about 6.5 and 7.0 ppm). The molar ratios were calculated by taking into account the integration of aniline aromatic peaks at 7.0 ppm and the characteristic peak of β-CD at about 4.46 ppm (OH-6) for the DMSO-d_6 system. The amount of aniline adsorbed was calculated from the content of β-CD, and the amount of aniline adsorbed by per unit mass of Janus membranes was further obtained. The results are summarized in Table 1. It was

Table 1. Amount of Aniline Adsorbed by Unit Mass of Janus Membranes Were Calculated from the ^{1}H NMR Spectra of the Janus Membranes after Aniline Exposure

Janus membranes	aniline (mg/g)
PAN/β-CD/PCL/ZnO	247.9
PAN/PCL/ZnO	168.4
PAN/β-CD/11% PCL/2% PCL	449.8
PAN/11% PCL/2% PCL	238.0
PAN/β-CD/mask	13.70
PAN/mask	10.69

https://dx.doi.org/10.1021/acsami.0c18526
ACS Appl. Mater. Interfaces 2021, 13, 3109−3118

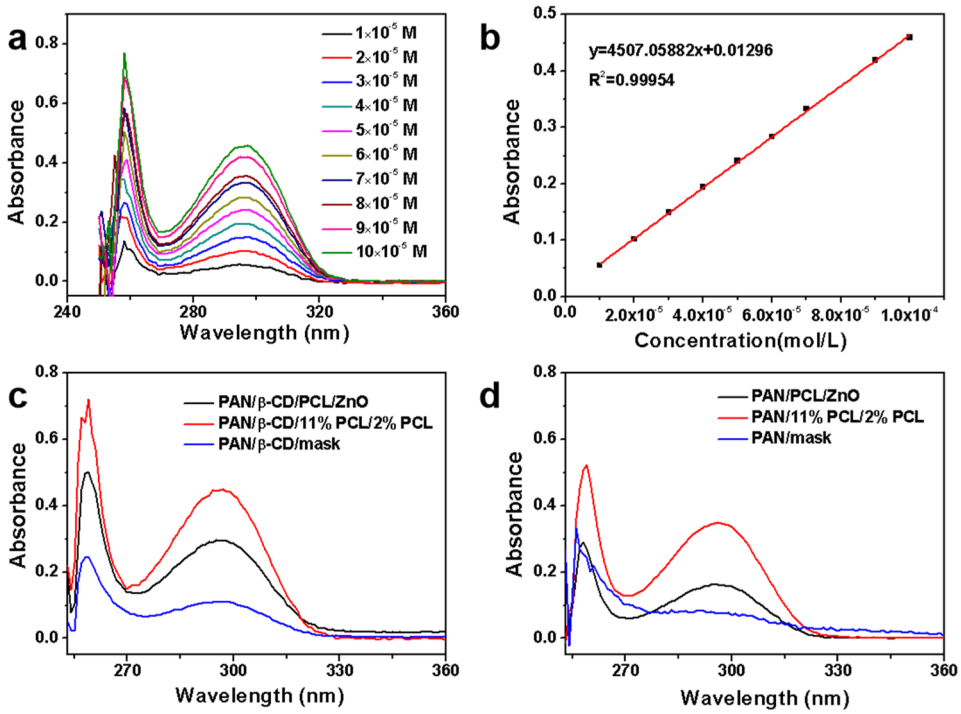

Figure 6. Janus membranes adsorb aniline efficiently. (a) Ultraviolet absorption curves of different concentrations of aniline in DMSO. (b) Absorbance of different concentrations of aniline in DMSO at 297 nm. The ultraviolet absorption curves of the Janus membranes (c) PAN/β-CD/PCL/ZnO, PAN/β-CD/11% PCL/2% PCL, and PAN/β-CD/mask and (d) PAN/PCL/ZnO, PAN/11% PCL/2% PCL, and PAN/mask dissolved in DMSO after adsorbing aniline.

observed that the amount of aniline adsorbed by per unit mass of PAN/β-CD/11% PCL/2% PCL (449.8 mg/g) is higher compared to PAN/11% PCL/2% PCL (238.0 mg/g); PAN/β-CD/PCL/ZnO (247.9 mg/g) is higher compared to PAN/PCL/ZnO (168.4 mg/g); and PAN/β-CD/mask (13.70 mg/g) is higher compared to PAN/mask (10.69 mg/g). The results indicated that the presence of β-CD increased the adsorption of aniline on the fibrous membranes because β-CD are capable of forming inclusion complexes with aniline due to their relatively hydrophobic cavity. In addition, there are many hydroxyl groups on β-CD, which can adsorb aniline through hydrogen bonding. The content of β-CD in PAN/β-CD/11% PCL/2% PCL, PAN/β-CD/PCL/ZnO, and PAN/β-CD/mask is about 45.11, 44.44, and 29.02%, respectively. So the order of aniline adsorption capacity is PAN/β-CD/11% PCL/2% PCL > PAN/β-CD/PCL/ZnO > PAN/β-CD/mask. All of the above results indicate that the β-CD in these Janus membranes plays an important role in the adsorption of aniline.

The adsorption performance of aniline was also tested by ultraviolet spectrophotometry. The results of UV detection are shown in Figure 6. The ultraviolet absorption spectra of aniline DMSO solutions with different concentrations were measured (Figure 6a), and then, a standard curve was drawn (Figure 6b). Then, Janus membranes adsorbed with aniline were dissolved in DMSO, and the ultraviolet absorption spectra were measured (Figure 6c,d).

By comparing the standard curve of aniline, the amount of aniline adsorbed by per unit mass of Janus membranes can be calculated. The results are summarized in Table 2. It is consistent with the results of ^{1}H NMR detection, the amount of aniline adsorbed by unit mass of PAN/β-CD/11% PCL/2% PCL (237.2 mg/g) is higher compared to PAN/11% PCL/2% PCL (166.2 mg/g); PAN/β-CD/PCL/ZnO (114.6 mg/g) is higher compared to PAN/PCL/ZnO (70.65 mg/g); and PAN/β-CD/mask (21.73 mg/g) is higher compared to PAN/mask (12.56 mg/g). The order of aniline adsorption capacity is PAN/β-CD/11% PCL/2% PCL > PAN/β-CD/PCL/ZnO > PAN/β-CD/mask.

Table 2. Amount of Aniline Adsorbed by Unit Mass of Janus Membranes Were Calculated from the UV−Vis Spectra of the Janus Membranes after Aniline Exposure

Janus membranes	aniline (mg/g)
PAN/β-CD/PCL/ZnO	114.6
PAN/PCL/ZnO	70.65
PAN/β-CD/11% PCL/2% PCL	237.2
PAN/11% PCL/2% PCL	166.2
PAN/β-CD/mask	21.73
PAN/mask	12.56

CONCLUSIONS

In summary, three Janus membranes of PAN/β-CD/PCL/ZnO, PAN/β-CD/11% PCL/2% PCL, and PAN/β-CD/mask have been successfully prepared. The water vapor or condensed water droplets exhaled by the human body could penetrate the membranes from hydrophobic PCL sides to hydrophilic PAN sides, then directed to the outside of the mask to reduce the uncomfortable feeling of dampness. The PM removal efficiency of PAN/β-CD/PCL/ZnO, PAN/β-CD/11% PCL/2% PCL, and PAN/β-CD/mask were 99.99, 99.98, and 91.56%, and the pressure drop of PAN/β-CD/PCL/ZnO, PAN/β-CD/11% PCL/2% PCL, and PAN/β-CD/mask was 156.5, 165.1, and 15.2 Pa, showing that besides high PM removal efficiency, the Janus membranes also maintain good air permeability. In addition, the Janus membranes with

https://dx.doi.org/10.1021/acsami.0c18526
ACS Appl. Mater. Interfaces 2021, 13, 3109−3118

highly porous structure could effectively adsorb VOCs in the porous structure of nanofibers or form inclusion complex with β-CD. The high PM removal efficiency, low airflow resistance, effective VOC adsorption, and great water unidirectional penetration performance make the obtained Janus nanofibrous membranes hopeful to be candidates for air filtration applications, especially for protective masks.

■ ASSOCIATED CONTENT

Supporting Information

The Supporting Information is available free of charge at https://pubs.acs.org/doi/10.1021/acsami.0c18526.

XRD patterns, stress−strain curves, N_2 adsorption/desorption isotherms and pore size distributions of Janus membranes, optical photographs of water transport performance and water vapor transmission rate test of Janus membranes, removal efficiency, pressure drop values and QF of Janus membranes, PM with different sizes before and after the filtration of Janus membranes, and ^{1}H NMR spectra of aniline-exposed Janus membranes (PDF)

Water penetrated the PAN/β-CD/PCL/ZnO Janus membrane from hydrophobic PCL/ZnO to hydrophilic PAN/β-CD direction (MP4)

Water blocked on the PAN/β-CD/PCL/ZnO Janus membrane from hydrophilic PAN/β-CD to hydrophobic PCL/ZnO direction (MP4)

Water penetrated the PAN/β-CD/11% PCL/2% PCL Janus membrane from hydrophobic 11% PCL/2% PCL to hydrophilic PAN/β-CD direction (MP4)

Water blocked on the PAN/β-CD/11% PCL/2% PCL Janus membrane from hydrophilic PAN/β-CD to hydrophobic 11% PCL/2% PCL direction (MP4)

Water penetrated the PAN/β- CD/mask Janus membrane from hydrophobic mask to hydrophilic PAN/β-CD direction (MP4)

Water blocked on the PAN/β-CD/mask Janus membrane from hydrophilic PAN/β-CD to hydrophobic mask direction (MP4)

■ AUTHOR INFORMATION

Corresponding Author

Yu Liu − *College of Chemistry, State Key Laboratory of Elemento-Organic Chemistry, Nankai University, Tianjin 300071, P. R. China;* orcid.org/0000-0001-8723-1896; Email: yuliu@nankai.edu.cn

Authors

Wenshi Xu − *College of Chemistry, State Key Laboratory of Elemento-Organic Chemistry, Nankai University, Tianjin 300071, P. R. China*

Yong Chen − *College of Chemistry, State Key Laboratory of Elemento-Organic Chemistry, Nankai University, Tianjin 300071, P. R. China*

Complete contact information is available at: https://pubs.acs.org/10.1021/acsami.0c18526

Author Contributions

Y.L., Y.C., and W.X. conceived and designed the experiments. W.X. conducted all experiments. W.X. wrote the main manuscript. Y.L. supervised the work and edited the manuscript. All authors analyzed and discussed the results and reviewed the manuscript.

Funding

This work was financially supported by the National Natural Science Foundation of China (grant nos. 21672113, 21772099, 21861132001, and 21971127).

Notes

The authors declare no competing financial interest.

■ ACKNOWLEDGMENTS

We thank National Natural Science Foundation of China (NNSFC) (grant nos. 21672113, 21772099, 21861132001, and 21971127) for financial support.

■ REFERENCES

(1) Raturi, R.; Prasad, J. R. Recognition of future air quality index using artificial neural network. *Int. J. Sci. Res. Dev.* **2018**, *6*, 1364.

(2) Ravindra, K.; Singh, T.; Mor, S.; Singh, V.; Mandal, T. K.; Bhatti, M. S.; Gahlawat, S. K.; Dhankhar, R.; Mor, S.; Beig, G. Real-time monitoring of air pollutants in seven cities of North India during crop residue burning and their relationship with meteorology and transboundary movement of air. *Sci. Total Environ.* **2019**, *690*, 717−729.

(3) Shehab, M. A.; Pope, F. D. Effects of short-term exposure to particulate matter air pollution on cognitive performance. *Sci. Rep.* **2019**, *9*, 8237.

(4) Wang, H.; Zhang, Y.; Zhao, H.; Lu, X.; Zhang, Y.; Zhu, W.; Nielsen, C. P.; Li, X.; Zhang, Q.; Bi, J.; McElroy, M. B. Trade-driven relocation of air pollution and health impacts in China. *Nat. Commun.* **2017**, *8*, 738.

(5) Machin, A. B.; Nascimento, L. F.; Mantovani, K.; Machin, E. B. Effects of exposure to fine particulate matter in elderly hospitalizations due to respiratory diseases in the South of the Brazilian Amazon. *Braz. J. Med. Biol. Res.* **2019**, *52*, No. e8130.

(6) Wang, L.; Xu, J.; Liu, H.; Li, J.; Hao, H. PM2.5 inhibits SOD1 expression by up-regulating microRNA-206 and promotes ROS accumulation and disease progression in asthmatic mice. *Int. Immunopharmacol.* **2019**, *76*, 105871.

(7) Duan, Y.; Liao, Y.; Li, H.; Yan, S.; Zhao, Z.; Yu, S.; Fu, Y.; Wang, Z.; Yin, P.; Cheng, J.; Jiang, H. Effect of changes in season and temperature on cardiovascular mortality associated with nitrogen dioxide air pollution in Shenzhen, China. *Sci. Total Environ.* **2019**, *697*, 134051.

(8) Krzeszowiak, J.; Pawlas, K. Particulate matter (PM2,5 and PM10), properties and epidemiological significance for respiratory and cardiovascular diseases. A review of the literature on the effects of short- and long-term exposure. *Med. Srodowiskowa* **2018**, *21*, 7−13.

(9) Calderón-Garcidueñas, L.; Gonzalez-Maciel, A.; Kulesza, R. J.; Gonzalez-Gonzalez, L. O.; Reynoso-Robles, R.; Mukherjee, P. S.; Torres-Jardon, R. Air Pollution, Combustion and Friction Derived Nanoparticles, and Alzheimer's Disease in Urban Children and Young Adults. *J. Alzheimer's Dis.* **2019**, *70*, 341−358.

(10) Cislaghi, C.; Nimis, P. L. Lichens, air pollution and lung cancer. *Nature* **1997**, *387*, 463−464.

(11) Guo, H.; Chang, Z.; Wu, J.; Li, W. Air pollution and lung cancer incidence in China: Who are faced with a greater effect? *Environ. Int.* **2019**, *132*, 105077.

(12) Kresovich, J. K.; Erdal, S.; Chen, H. Y.; Gann, P. H.; Argos, M.; Rauscher, G. H. Metallic air pollutants and breast cancer heterogeneity. *Environ. Res.* **2019**, *177*, 108639.

(13) Xu, W.; Chen, Y.; Xu, W.; Wu, X.; Liu, Y. Electrospinning Oriented Self-Cleaning Porous Crosslinking Polymer for Efficient Dyes Removal. *Adv. Mater. Interfaces* **2020**, *7*, 2001050.

(14) Jing, L.; Shim, K.; Toe, C. Y.; Fang, T.; Zhao, C.; Amal, R.; Sun, K.-N.; Kim, J. H.; Ng, Y. H. Electrospun Polyacrylonitrile-Ionic Liquid Nanofibers for Superior PM2.5 Capture Capacity. *ACS Appl. Mater. Interfaces* **2016**, *8*, 7030−7036.

(15) Wang, X.; Xu, W.; Gu, J. g.; Yan, X.; Chen, Y.; Guo, M.; Zhou, G.; Tong, S.; Ge, M.; Liu, Y.; Chen, C. MOF-based fibrous membranes adsorb PM efficiently and capture toxic gases selectively. *Nanoscale* **2019**, *11*, 17782−17790.
(16) Li, Q.; Xu, Y.; Wei, H.; Wang, X. An electrospun polycarbonate nanofibrous membrane for high efficiency particulate matter filtration. *RSC Adv.* **2016**, *6*, 65275−65281.
(17) Zhang, B.; Zhang, Z.-G.; Yan, X.; Wang, X.-X.; Zhao, H.; Guo, J.; Feng, J.-Y.; Long, Y.-Z. Chitosan nanostructures by in situ electrospinning for high-efficiency PM2.5 capture. *Nanoscale* **2017**, *9*, 4154−4161.
(18) Xu, W.; Guo, M.; Liu, J.; Xiao, Y.; Zhou, G.; Liu, Y.; Chen, C. Poly(lactic-co-glycolic acid)/polycaprolactone nanofibrous membranes for high-efficient capture of nano- and microsized particulate matter. *J. Biomed. Nanotechnol.* **2018**, *14*, 179−189.
(19) Huang, X.; Jiao, T.; Liu, Q.; Zhang, L.; Zhou, J.; Li, B.; Peng, Q. Hierarchical electrospun nanofibers treated by solvent vapor annealing as air filtration mat for high-efficiency PM2.5 capture. *Sci. China Mater.* **2019**, *62*, 423−436.
(20) Ge, J.; Choi, N. J. Fabrication of functional polyurethane/rare earth nanocomposite membranes by electrospinning and its VOCs absorption capacity from air. *Nanomaterials* **2017**, *7*, 60.
(21) Liu, C.; Hsu, P.-C.; Lee, H.-W.; Ye, M.; Zheng, G.; Liu, N.; Li, W.; Cui, Y. Transparent air filter for high-efficiency PM2.5 capture. *Nat. Commun.* **2015**, *6*, 6205.
(22) Alzate-Sánchez, D. M.; Smith, B. J.; Alsbaiee, A.; Hinestroza, J. P.; Dichtel, W. R. Cotton Fabric Functionalized with a beta-Cyclodextrin Polymer Captures Organic Pollutants from Contaminated Air and Water. *Chem. Mater.* **2016**, *28*, 8340−8346.
(23) Dai, L.; Wu, W.; Liang, W.; Chen, W.; Yu, X.; Ji, J.; Xiao, C.; Yang, C. Enhanced chiral recognition by γ-cyclodextrin-cucurbit[6]-uril-cowheeled [4]pseudorotaxanes. *Chem. Commun.* **2018**, *54*, 2643−2646.
(24) Fan, C.; Wu, W.; Chruma, J. J.; Zhao, J.; Yang, C. Enhanced Triplet−Triplet Energy Transfer and Upconversion Fluorescence through Host−Guest Complexation. *J. Am. Chem. Soc.* **2016**, *138*, 15405−15412.
(25) Li, D.; Lu, F.; Wang, J.; Hu, W.; Cao, X.-M.; Ma, X.; Tian, H. Amorphous Metal-Free Room-Temperature Phosphorescent Small Molecules with Multicolor Photoluminescence via a Host-Guest and Dual-Emission Strategy. *J. Am. Chem. Soc.* **2018**, *140*, 1916−1923.
(26) Zhang, Q.-W.; Li, D.; Li, X.; White, P. B.; Mecinović, J.; Ma, X.; Ågren, H.; Nolte, R. J. M.; Tian, H. Multicolor Photoluminescence Including White-Light Emission by a Single Host-Guest Complex. *J. Am. Chem. Soc.* **2016**, *138*, 13541−13550.
(27) Hao, M.; Sun, G.; Zuo, M.; Xu, Z.; Chen, Y.; Hu, X. Y.; Wang, L. A Supramolecular Artificial Light-Harvesting System with Two-Step Sequential Energy Transfer for Photochemical Catalysis. *Angew. Chem., Int. Ed.* **2020**, *59*, 10095−10100.
(28) Tian, J.; Xu, Z.-Y.; Zhang, D.-W.; Wang, H.; Xie, S.-H.; Xu, D.-W.; Ren, Y.-H.; Wang, H.; Liu, Y.; Li, Z.-T. Supramolecular metal-organic frameworks that display high homogeneous and heterogeneous photocatalytic activity for H_2 production. *Nat. Commun.* **2016**, *7*, 11580.
(29) Xiao, T.; Qi, L.; Zhong, W.; Lin, C.; Wang, R.; Wang, L. Stimuli-responsive nanocarriers constructed from pillar n arene-based supra-amphiphiles. *Mater. Chem. Front.* **2019**, *3*, 1973−1993.
(30) Phua, S. Z. F.; Xue, C.; Lim, W. Q.; Yang, G.; Chen, H.; Zhang, Y.; Wijaya, C. F.; Luo, Z.; Zhao, Y. Light-Responsive Prodrug-Based Supramolecular Nanosystems for Site-Specific Combination Therapy of Cancer. *Chem. Mater.* **2019**, *31*, 3349−3358.
(31) Wu, J.-R.; Yang, Y.-W. Synthetic Macrocycle-Based Nonporous Adaptive Crystals for Molecular Separation. *Angew. Chem., Int. Ed.* **2020**, *59*, 2−14.
(32) Celebioglu, A.; Huseyin, S. S.; Engin, D.; Tamer, U. Molecular entrapment of volatile organic compounds (VOCs) by electrospun cyclodextrin nanofibers. *Chemosphere* **2016**, *144*, 736−744.
(33) Wang, H.; Zhou, H.; Niu, H.; Zhang, J.; Du, Y.; Lin, T. Dual-Layer Superamphiphobic/Superhydrophobic-Oleophilic Nanofibrous Membranes with Unidirectional Oil-Transport Ability and Strengthened Oil-Water Separation Performance. *Adv. Mater. Interfaces* **2015**, *2*, 1400506.
(34) Shi, L.; Liu, X.; Wang, W.; Jiang, L.; Wang, S. A Self-Pumping Dressing for Draining Excessive Biofluid around Wounds. *Adv. Mater.* **2019**, *31*, 1804187.
(35) Dai, B.; Li, K.; Shi, L.; Wan, X.; Liu, X.; Zhang, F.; Jiang, L.; Wang, S. Bioinspired Janus Textile with Conical Micropores for Human Body Moisture and Thermal Management. *Adv. Mater.* **2019**, *31*, 1904113.
(36) Zhao, R.; Wang, Y.; Li, X.; Sun, B.; Wang, C. Synthesis of beta-Cyclodextrin-Based Electrospun Nanofiber Membranes for Highly Efficient Adsorption and Separation of Methylene Blue. *ACS Appl. Mater. Interfaces* **2015**, *7*, 26649−26657.
(37) Wu, J.; Wang, N.; Wang, L.; Dong, H.; Zhao, Y.; Jiang, L. Unidirectional water-penetration composite fibrous film via electrospinning. *Soft Matter* **2012**, *8*, 5996−5999.
(38) Hou, L.; Wang, N.; Man, X.; Cui, Z.; Wu, J.; Liu, J.; Li, S.; Gao, Y.; Li, D.; Jiang, L.; Zhao, Y. Interpenetrating Janus Membrane for High Rectification Ratio Liquid Unidirectional Penetration. *ACS Nano* **2019**, *13*, 4124−4132.

https://dx.doi.org/10.1021/acsami.0c18526
ACS Appl. Mater. Interfaces 2021, 13, 3109−3118